Simulation of Water Adsorption on Kaolinite under Atmospheric Conditions

T. Croteau, A. K. Bertram,* and G. N. Patey†

Department of Chemistry, University of British Columbia, Vancouver, British Columbia, Canada V6T 1Z1

Received: March 18, 2009; Revised Manuscript Received: May 7, 2009

Grand canonical Monte Carlo calculations are employed to investigate water adsorption on kaolinite at 298 and 235 K. Both basal planes (the Al and Si surfaces) as well as two edge-like surfaces are considered. The general force field CLAYFF is used together with the SPC/E and TIP5P-E models for water. Problems that occur in single slab simulations due to arbitrary truncation of the point charge lattice are identified, and a working remedy is discussed. The edges and the Al surface adsorb water at subsaturation in the atmospherically relevant pressure range. The Si surface remains dry up to saturation. Both edges have a very strong affinity for water and adsorb continuously up to monolayer coverage. The Al surface has a weaker affinity for water but forms a subsaturation monolayer. On the Al surface, the monolayer is formed in an essentially sharp transition, and strong hysteresis is observed upon desorption. This indicates collective behavior among the water molecules which is not present for the edges. Binding energies of singly adsorbed water molecules at 10 K were determined to understand the differences in water uptake by the four kaolinite surfaces. Binding energies (SPC/E) of −21.6, −46.4, −73.5, and −94.1 kJ/mol, were determined for the Si surface, Al surface, unprotonated edge, and protonated edge, respectively. The water monolayer on the Al surface, particularly at 235 K, exhibits hexagonal patterns. However, the associated lattice parameters are not compatible with ice *Ih*. Water density and hydrogen bonding in the monolayers at both 298 and 235 K were also determined to better understand the structure of the adsorbed water.

I. Introduction

Mineral dust particles are abundant in the atmosphere, with estimated total global emissions of 800−1500 Tg/year.[1−5] The components of aerosolized mineral dust found in the atmosphere include illite, kaolinite, montmorillonite, quartz, and calcite. Kaolinite represents a significant component, comprising approximately 5−10% of aerosolized mineral dust.[6] In the atmosphere, mineral dust particles can take up water and act as cloud condensation nuclei or ice nuclei.[7−13] Thus, mineral dust particles can influence climate by changing the frequency and properties of clouds.[8,10,14,15] To completely understand these processes, one must first understand the interaction of water with mineral dust particles.

Mineral dust particles can also provide a surface on which heterogeneous reactions can occur in the atmosphere. These reactions could be a sink of gas-phase atmospheric species and influence the chemical composition of the mineral dust particles.[16] Examples of reactions that may occur on mineral dust particles are the hydrolysis of N_2O_5 and the uptake of HNO_3. Recent studies[17−23] have shown that these reactions can be strongly influenced by the presence of water on mineral surfaces. Hence, in order to understand these reactions under atmospheric conditions, an understanding of the interaction of water with mineral surfaces is also necessary.

One method of studying the interaction of water with mineral surfaces is to use computational methods. The interaction of water with kaolinite has been investigated in several ab initio studies, which have confirmed the hydrophobic and hydrophilic nature of the Si and Al surfaces, respectively.[24−28] The hydrophobicity of the Si surface refers to its rather weak interaction with a water molecule, which, in some instances, can lead to water clustering instead of layering.

The recent computational studies of Hu and Michaelides[27,28] are of particular relevance for ice nucleation studies. These authors have examined water on the Al surface of kaolinite by employing density functional theory (DFT). They found that a two-dimensional (2D) water layer with a stability comparable to that of ice *Ih* could be formed on the Al surface, but they note a mismatch between the ice *Ih* lattice and the 2D water structure imposed by the substrate. Moreover, they note that multilayers of water on the Al surface are less stable than bulk ice.

More recently, we used grand canonical Monte Carlo (GCMC) calculations to study water adsorption and structure on kaolinite surfaces as a function of relative humidity (RH) at 235 K, with a focus on ice nucleation.[29] We found monolayer formation, but the lattice parameters did not match that of ice *Ih*. Indeed, the strain produced on an ice embryo by the lattice mismatch strongly suggests that an atomically smooth, defect-free Al surface would not be a good ice nucleus, contrary to some previous speculation.[30]

There have been a number of simulation studies of water on various related surfaces, including the Al and Si surfaces of kaolinite,[31−33] CaF_2 and BaF_2,[34] β-AgI,[35−37] metals,[38,39] and model hexagonal surfaces.[40] However, we note that the vast majority of this work has employed closed systems and does not address adsorption questions. A relevant exception is the work of Delville,[33] who focused on the Si surface.

The present paper describes a significant extension of our initial studies of water adsorption on kaolinite at 235 K, which focused on ice nucleation.[29] Here, we investigate in detail water adsorption on kaolinite at both 298 and 235 K, again employing the GCMC method, which is well-suited to address adsorption questions. The calculations at 298 K allow us to compare

* To whom correspondence should be addressed. E-mail: bertram@chem.ubc.ca.

† E-mail: patey@chem.ubc.ca.

10.1021/jp902453f CCC: $40.75
Published on Web 06/10/2009

qualitatively with recent adsorption experiments,[41] and those at 235 K are motivated by ice nucleation experiments carried out at that temperature.[9,10] Four kaolinite surfaces are considered. These include the hydrophilic Al surface, the hydrophobic Si surface, and two so-called edge configurations (defined below). Some of the topics addressed in the present paper that were not included in our preliminary report are as follows.

We examine the modeling/simulation techniques employed and identify potential problems that can arise. For example, we note that arbitrary truncation of a kaolinite slab (a lattice of point charges) can lead to strong unphysical fields at long distances from the surface of interest. These fields can seriously distort the results obtained, but we show that such effects can be essentially eliminated by carrying out simulations with two slabs arranged such that the long-range, truncation-dependent fields cancel exactly. We also examine the convergence of the Ewald sums necessary to take account of the long-range Coulombic interactions.

We determine water adsorption isotherms at 298 and 235 K for all four surfaces, and the results are compared with recent laboratory studies. We study the orientation and binding energies of single adsorbed water molecules at 10 K to understand the differences in water uptake by the four kaolinite surfaces. This includes determination of the binding energies and geometric arrangements of single water molecules on the surface, as well as water−surface hydrogen bond analyses. The water structure in the monolayers is analyzed using density and hydrogen-bond number profiles.

The remainder of this paper is organized into three parts. The models and simulation issues are discussed in section II, the results are presented and discussed in section III, and our conclusions are summarized in section IV.

II. Model and Method

The model used for the clay lattice is CLAYFF, a general force field developed by Cygan et al.[42] In this model, the short-range interactions of all atoms are represented by Lennard-Jones (LJ) potentials. For the lattice oxygens, the parameters assigned are identical to those of the single point charge (SPC) model for water.[43] Partial charges for all lattice atoms were derived by periodic density functional theory calculations based on the electronic structures of simple oxides and hydroxides (e.g., quartz (α-SiO_2), corundum (α-Al_2O_3), boehmite (γ-AlO(OH)), and others).[42] The structure of kaolinite obtained by Bish[44] was used to improve the optimization of the interaction parameters. The versatility of this model, mainly due to the use of a nonbonded description for the interatomic interactions of the lattice, gives a general force field suitable for application to a wide variety of different clays. To keep the computational requirements practical, we use a rigid lattice corresponding to the most stable kaolinite configuration.[44]

We employ the extended single point charge SPC/E[45] and TIP5P-E[46] models to represent the water−water and water−lattice interactions. The SPC/E is a widely used three-site model with the Coulombic interactions described by three point charges (one for each atomic nucleus) embedded in a LJ sphere centered at the oxygen. TIP5P-E is a recent reparameterization of the original TIP5P model[47] to better treat the long-range interactions when using Ewald sums. It is a five-site model with positive charges located at the hydrogen nuclei and negative charges at "lone pair" positions, all embedded in a LJ sphere centered at the oxygen nucleus. The water models are rigid with oxygen−hydrogen bond lengths of 1 and 0.9572 Å, and bond angles of 109.47 and 104.52° for the SPC/E and TIP5P-E models, respectively. For TIP5P-E, the oxygen lone pairs are located at 0.7 Å, with a bond angle of 109.47°. Both models give a reasonably good description of water structure and properties[45,48] under ambient conditions. We note that the TIP5P-E model gives a more accurate prediction of the melting point of ice, 274 compared with 215 K for the SPC/E model.[49] However, this difference does not appear to have a significant influence on water adsorption on kaolinite. Two different water models are used to ensure as far as possible that model-dependent effects are not significantly influencing our observations and conclusions. It should be noted that both water models employed are rigid point-charge models that do not allow for water dissociation. While water dissociation might play a significant role in surface chemistry, we would not expect it to have a large influence on the adsorption isotherms.

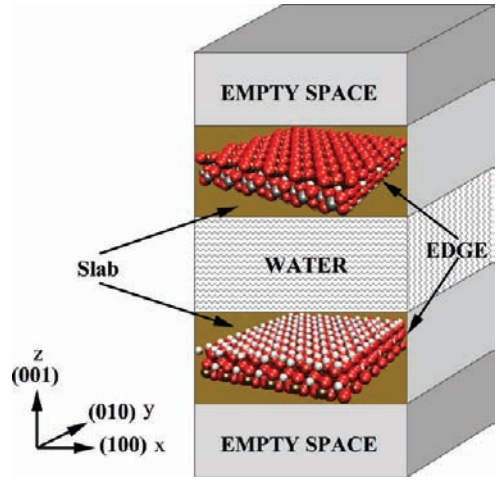

Figure 1. The simulation cell.

The configurational energy for our system, U, is given by the sum of Coulombic and LJ interactions

$$U = \frac{e^2}{4\pi\epsilon_o}\sum_{i\neq j}\frac{q_i q_j}{r_{ij}} + \sum_{i\neq j} D_{o,ij}\left[\left(\frac{R_{o,ij}}{r_{ij}}\right)^{12} - 2\left(\frac{R_{o,ij}}{r_{ij}}\right)^{6}\right] \quad (1)$$

where the sums are over all lattice and water interaction sites and r_{ij} is the distance between sites i and j. The first term represents the Coulombic interactions, where q_i is the point charge on site i, e is an elementary charge, and ϵ_o is the dielectric permittivity of free space. The second term represents the LJ contribution, and the energy and distance parameters for the different site−site interactions, $D_{o,ij}$ and $R_{o,ij}$, respectively, are given in ref 42. For the cross interactions, the Lorentz−Berthelot rules, $D_{o,12} = (D_{o,11}D_{o,22})^{1/2}$ and $R_{o,12} = (R_{o,11} + R_{o,22})/2$, are used.

Kaolinite [$Al_2Si_2O_5(OH)_4$] is a clay mineral that has a layered structure. These layers consist of octahedral aluminum (Al surface) and tetrahedral silicon (Si surface). Kaolinite consists of many of these layers attached together by hydrogen bonds between the hydroxyl groups extending from the Al surface and bridging oxygens on the Si surface. The large number of hydrogen bonds connecting the layers makes them almost inseparable. Thus, kaolinite is described as a nonexpanding or nonswelling clay. The three-dimensional simulation cell illustrated in Figure 1 is constructed such that the Al and Si surfaces are parallel to the (001) plane. The rectangular lattices periodically replicated in the xy plane are composed of 48

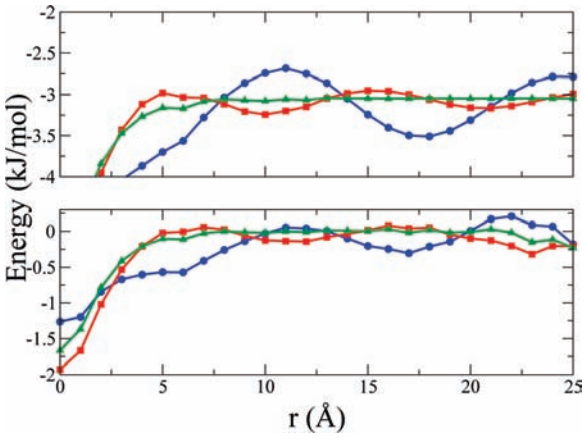

Figure 2. The surface−water interaction energy of a single, randomly oriented, SPC/E water molecule as a function of the perpendicular distance from the center of the highest hydroxyl hydrogen atom on the Al surface. The top and bottom panels show the results obtained for simulation cells with one and two slabs, respectively. The blue (circles), red (squares), and green (triangles) lines correspond to 6858, 15624, and 226980 *k*-space wave vectors, respectively.

kaolinite unit cells for a total of 816 atoms per surface. The *x* and *y* dimensions of the cell are 30.921 and 35.7676 Å, respectively.

In addition to the Al and Si surfaces, we consider two additional surfaces that commonly occur in kaolinite samples[50−52] and are sometimes called "edges", a term that we will adopt here. Two extreme edge cases are considered, one which has "bare" oxygens exposed (unprotonated edge) and another where all oxygens are protonated (protonated edge). The unprotonated edge is constructed by cleaving the Al surface along the (100) plane such as to have oxygen atoms exposed (see Figure 1). The surface is then rotated 90° counterclockwise to bring the exposed oxygens into the (001) plane and expanded to have *x* and *y* dimensions of 29.524 and 35.76764 Å, respectively, and contain 816 atoms. A protonated edge is constructed by placing hydrogen atoms (a total of 64), each with a charge of 0.4250e, 1 Å above every bare oxygen atom. To counterbalance this extra charge and maintain a neutral surface, an opposing negative charge is equally distributed on all sites below the first layer of Al and Si atoms. Specifically, a negative charge of 0.05e is placed on all 544 sites below the surface. This procedure is obviously somewhat arbitrary, but changing the surface thickness (thus reducing the charge per subsurface site) does not have any significant effect on the results obtained. We remark that many "edge" surfaces could be constructed by cleaving kaolinite along different planes. The particular edges considered here have been discussed by previous authors[50−52] and are believed to make a significant contribution to the surface area of kaolinite samples.

Care must be taken in simulating slabs that are periodically infinite in two dimensions (*x* and *y*) but arbitrarily truncated in the third (*z*). Although our samples are overall electrically neutral, arbitrary truncation of the discrete point charge lattice can induce local charge imbalance at the resulting surface and significant net polarization. This can create unphysical fields that depend strongly on the slab thickness and can act at large distances from the surface. Such effects would not occur for an infinitely thick sample because charges in neighboring layers preserve local charge neutrality. As an illustration of the problem, the interaction energy of a water molecule (arbitrary orientation) with a single surface is shown in Figure 2 (top). We note that the interaction energy does not decay quickly and is about −3 kJ/mol at a distance of 25 Å from the surface. This unphysical interaction strongly depends on the slab thickness, is different for different surfaces, and can significantly influence the results obtained. For example, for the Al and Si surfaces, one can observe small isolated water "towers" on the surface, such as those previously reported by Delville[33] for the Si surface. We believe that such effects are artifacts of the long-range, unphysical field resulting from truncation of the charge lattice. One way to solve this problem is to add an opposing surface having the same size and layer structure (see Figure 1), such that the unphysical fields produced by truncation simply cancel. We note that this technique was previously employed by Warne and Cosgrove[31] for similar reasons. Results for a single water molecule in a two-slab arrangement are also shown in Figure 2, and we see that the interaction now approaches 0 at about 10 Å from the surface. The strong dependence on slab thickness (not shown) found for a single slab vanishes when two slabs are used. Furthermore, unusual structures such as isolated water towers without any obvious physical explanation no longer occur.

The configurational energies were obtained using a method previously applied to slab geometries with long-range electrostatic interactions.[53,54] We wish to calculate the long-range interactions in a slab of finite thickness. One way to do this is to periodically repeat the cell shown in Figure 1 in three dimensions and apply the usual 3D Ewald method[55] but leave enough empty space to prevent the undesired images in the *z* direction from having a significant physical influence.[53,54] For our systems, an empty gap of 107 Å was found to be sufficient for this purpose, and increasing the gap further had no noticeable effect. Comparing adsorption results, it was judged sufficient to employ 6858 wave vectors in the Ewald sums as no significant change was observed with larger numbers. The other Ewald parameters employed were $\alpha = 0.175$ Å^{-1} and a reciprocal space cutoff of 2.0 Å^{-1}. The LJ and real space interactions were cut off at half of the length of the *x* side of the simulation cell.

The simulations were carried out employing the GCMC method.[55] This method allows the equilibrium properties of an open system to be obtained at fixed chemical potential, μ, volume, and temperature. In the present calculations, the number of water molecules, N_W, fluctuates. A Monte Carlo step is defined as an attempted insertion, deletion, or displacement (rotation or translation) of a water molecule, and all three possibilities were attempted with equal probability. The acceptance rate for insertion (deletion) moves was ∼0.01%, which is comparable to that found in GCMC simulations of bulk water;[56] the maximum size of the displacement moves was adjusted to give an acceptance rate of ∼50%. To ensure convergence, the systems were equilibrated for at least 5×10^7 Monte Carlo (MC) steps. Following equilibration, averages were collected for 2×10^8 or more MC steps and include energy, water content, density profile, and hydrogen-bond number. This procedure was repeated for a wide range of chemical potentials and at different temperatures to produce adsorption isotherms and related properties for all four surfaces.

For the two-slab geometry discussed above (Figure 1), the number of layers included in each kaolinite slab did not significantly influence the results, and a single layer (constructed as described above) was sufficient for this investigation. However, since we are interested in modeling adsorption on single surfaces rather than in slits of finite width, care must be taken to place the slabs sufficiently far apart such that the water adsorption on each slab is not influenced by the presence of the other. Most simulations were carried out with the slabs

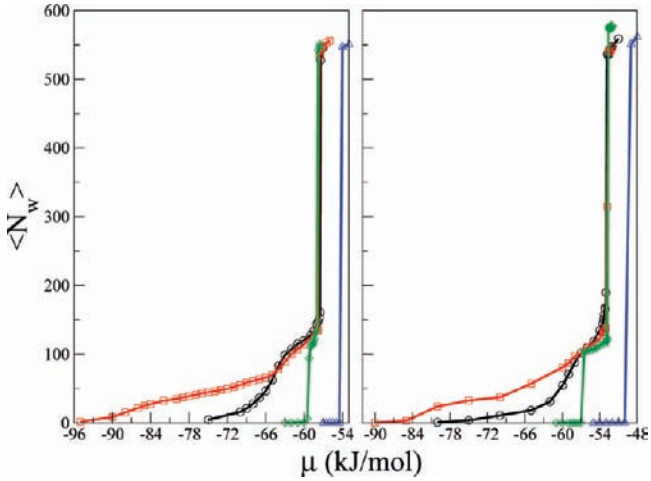

Figure 3. Adsorption isotherms at 298 K for the four surfaces considered, obtained with a slab separation of 30 Å. Results for the SPC/E (left) and TIP5P-E (right) models are shown. The black (circles), red (squares), green (diamonds), and blue (triangles) curves correspond to the unprotonated edge, protonated edge, Al surface, and Si surface, respectively.

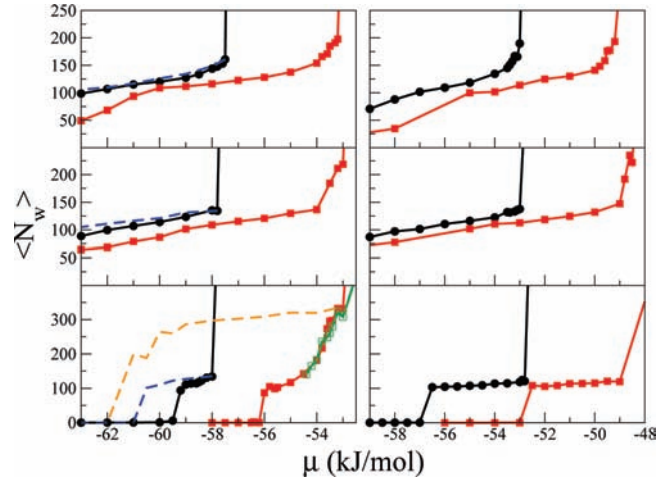

Figure 4. Adsorption isotherms obtained for the unprotonated edge (top panel), the protonated edge (middle panel), and the Al surface (bottom panel) using SPC/E (left) and TIP5P-E (right) models at 298 (black curves with filled circles) and 235 K (red curves with filled squares). The green curve with empty squares was obtained at 235 K with a slab separation of 60 Å. All other curves were obtained with a slab separation of 30 Å. The blue and yellow dashed curves are desorption isotherms.

separated by 30 Å, but some test runs were performed with a separation of 60 Å. These confirmed that, at least before the filling transition at saturation (bulk condensation of the vapor), the surfaces adsorbed independently. The results reported were obtained by averaging values for both surfaces, which improves the statistics. Some simulations were also performed by varying the x and y cell dimensions by factors of 0.5 and 1.5, and again, these tests revealed no significant system size dependence.

III. Results and Discussion

A. Water Adsorption at 298 and 235 K. Adsorption isotherms for all four surfaces obtained at 298 K are displayed in Figure 3 as a function of chemical potential. The water coverage plotted on the vertical axis is the average number of water molecules adsorbed on a single surface. For atmospheric comparisons, it is often useful to convert the chemical potential scale into pressure/saturated vapor pressure (P/P_o). Since the saturated vapor pressure of water at 298 and 235 K is low (<0.1 atm), the vapor pressures can be estimated using the ideal gas relationship, $P = e^{\beta\mu_{tr}}/\beta\Lambda^3$, where μ_{tr} is the translational contribution to the chemical potential and Λ is the thermal de Broglie wavelength. The saturated vapor pressure P_o for our models can be found by setting $P/P_o = 1$ at the filling transitions observed in the simulations. Some P/P_o estimates are given below. In contrast to the Al surface and the edges, for both water models considered, the Si surface remains completely dry up to the filling transition. For this reason, no further adsorption results are presented for the Si surface.

Qualitatively similar adsorption behavior is observed for both water models. Both edges adsorb readily even at low chemical potentials (vapor pressures), the protonated edge having the greatest affinity for water. Adsorption begins at very low chemical potentials for these surfaces, that is, below $\mu \approx -75.0$ ($P/P_o \approx 9.6 \times 10^{-4}$) and -90.0 kJ/mol ($P/P_o \approx 2.3 \times 10^{-6}$) for the unprotonated and protonated edges, respectively. As the chemical potential is increased, the water uptake increases slowly, partially covering the surface at well-defined binding sites (see discussion below) until a monolayer is obtained at $\mu \approx -63.0$ kJ/mol ($P/P_o \approx 0.12$)(SPC/E). The film then thickens, and finally, a transition to a completely filled state occurs. The strong water affinity of the edges demonstrates that they can make an important contribution to water uptake and could well play an important role in heterogeneous surface chemistry that involves water.

In contrast, adsorption on the Al surface occurs over a much narrower range of chemical potentials (which is slightly larger for TIP5P-E), suggesting a weaker water affinity on that surface. On the chemical potential scale shown in Figure 3, it is only just prior to filling, at $\mu \approx -59.2$ (SPC/E) and -56.5 kJ/mol (TIP5P-E), that monolayer coverage is achieved. Note that we take monolayer coverage to be a density of one water molecule per 9 Å^2 of surface area (assuming a smooth surface) or about 100 molecules on a single surface in our simulation cell. In terms of the relative vapor pressure, P/P_o, the adsorption range on the Al surface is of atmospheric relevance. The P/P_o range over which adsorption occurs is approximately 0.55−1 at 298 K, and 0.2−1 at 235 K, which covers the range of interest for atmospheric science.[14]

For all surfaces considered, adsorption isotherms at 235 K exhibit trends similar to those described above for 298 K. A comparison is made in Figure 4, where results obtained at 298 and 235 K are plotted for both edges and the Al surface. For all three surfaces, the overall shape of the adsorption isotherms is similar at both temperatures. As noted above, the Al surface takes up water just before filling occurs, and both edges adsorb water readily at low chemical potentials. The thickness achieved by the water films before filling does show some variation with temperature, particularly for the SPC/E model. At 235 K, the edges acquire slightly thicker films before the filling transition occurs, at $\mu \approx -54.0$ kJ/mol for SPC/E and $\mu \approx -49.0$ kJ/mol for TIP5P-E. On the Al surface, there is a significant difference between the SPC/E and TIP5P-E models. The TIP5P-E model shows no increase in film thickness before filling when the temperature is reduced from 298 to 235 K. However, the SPC/E model exhibits an increase in thickness, forming essentially a bilayer just prior to filling. To check that this increased thickness is not associated with the two-slab geometry, simulations were performed with the Al surfaces separated by 60 Å. The results obtained are also shown in Figure 4 (bottom panel) and verify that the additional thickening observed at 235 K is not related to interactions with the second surface.

TABLE 1: Binding Energies and Hydrogen-Bond Numbers for Single Water Molecules Obtained Using NVT Monte Carlo Simulations at 10 K[a]

surface type	water−surface hydrogen bonds		$\langle U_{water-surface} \rangle$ (kJ/mol)	
water model	SPC/E	TIP5P-E	SPC/E	TIP5P-E
Si surface	1	0	−21.64(0.03)	−21.03(0.04)
Al surface	3	1	−46.36(0.04)	−45.64(0.02)
unprotonated edge	1	1	−73.45(0.02)	−71.42(0.03)
protonated edge	2	2	−94.14(0.02)	−78.51(0.04)

[a] The numbers in brackets represent one standard deviation.

Some associated desorption isotherms for the SPC/E model are also plotted in Figure 4. These were obtained by carrying out simulations at decreasing chemical potentials, starting with an initial configuration obtained at a chemical potential that is just below the filling transition on the adsorption curve. Simulations were carried out at decreasing chemical potentials until all water molecules evaporated. We noted above that adsorption on the edges is relatively smooth before the filling transition. This, together with the fact that the desorption curves reveal relatively little hysteresis, suggests that water adsorption on the edges is essentially a continuous process, dominated by water−surface interactions. In contrast, water adsorption on the Al surface is not smooth and "jumps" rather sharply from essentially nothing to monolayer coverage. Additionally, the desorption curves show a large hysteresis at both temperatures. These observations indicate that water adsorption on the Al surface has strong "first-order" characteristics, with important collective behavior among the water molecules.

Recently, Schuttlefield et al.[41] investigated water uptake on kaolinite minerals using ATR-FTIR spectroscopy coupled with quartz crystal microbalance measurements at 296 K. The data show that kaolinite particles take up water continuously from 0 to 90% RH ($P/P_o \times 100$). At a RH of 50%, they observed approximately 6−25 monolayers of water uptake, and at 80% RH, they observed approximately 10−40 monolayers of water uptake, depending on the source of the kaolinite. This is in contrast to our simulations at 298 K, where we do not observe more than approximately monolayer coverage below 100% RH for any of the surfaces considered. The simulations suggest that the water uptake observed in the laboratory experiments cannot be explained by water uptake on defect-free surfaces.

B. Orientations and Binding Energies of Singly Adsorbed Water Molecules. The differences in water uptake by the four kaolinite surfaces can be largely understood by considering the low-temperature water−surface binding energies. Results obtained in NVT Monte Carlo simulations at 10 K involving only a single water molecule are summarized in Table 1. The standard deviations included in Table 1 were obtained by dividing Monte Carlo runs of 10^6 steps into 10 equal blocks and assuming that the block averages are independent estimates of the water−surface interaction energy. Other error estimates using widely spaced single configuration energies gave similar values. We note that the average water−surface energies obtained for the SPC/E and TIP5P-E models are in good agreement, except for the protonated edge, where the SPC/E interaction is more attractive by ∼15.6 kJ/mol. For both models, the single water molecule binding energies correlate well with the water adsorption curves shown in Figures 3 and 4. The weakest interaction is obtained for the Si surface which does not adsorb water before the chemical potential reaches bulk saturation, and the strongest interactions are for the edges which adsorb at very low chemical potentials (vapor pressures). In this case, the very strong water−surface interactions can support very low coverages both at 298 and 235 K. For the Al surface, which adsorbs near bulk saturation but in the atmospherically relevant range, the interaction energy lies between the two extremes. For the Al surface, the direct water−surface interaction is not strong enough for significant submonolayer coverage, and collective water−water interactions are necessary to stabilize the monolayer. This explains the relative sharpness of the transitions on this surface (Figures 3 and 4) and the hysteresis noted above.

It is instructive to consider the surface−single-water-molecule interactions in more detail. The geometric arrangements obtained at 10 K are shown in Figure 5, indicating clearly the clay atoms that form hydrogen bonds with the water molecule. We define a hydrogen bond using geometric criteria similar to those applied in earlier work.[57,58] Specifically, a water−water hydrogen bond is said to exist if and only if the water-oxygen−water-oxygen distance is less than 3.41 Å, the water-hydrogen−water-oxygen distance is less than 2.38 Å, and the O−O−H angle is less than 35°. This definition can be generalized to water−surface hydrogen bonds in an obvious manner. The lengths and angle chosen are clearly arbitrary to some extent, and using different parameters might, in some cases, influence the number of hydrogen bonds counted. In the present case, the number of water−surface hydrogen bonds is somewhat sensitive to the angle used, but 35° appears to be a reasonable choice yielding hydrogen-bond numbers consistent with those previously reported for the Al surface (see below).

We first consider the Si surface which has the weakest interaction with water. We note that the energies obtained for both water models are very similar despite the differing orientations (Figure 5a and b). For the SPC/E model (Figure 5a), there is a strong hydrogen bond between the water hydrogen and the closest bridging oxygen of the surface. The water hydrogens also have strong attractive interactions with other neighboring bridging oxygens. However, the structure shown in Figure 5a leads to highly repulsive interactions between the water hydrogens and silicon atoms of the surface, leading to a net attraction that is relatively weak. For the TIP5P-E model, the most attractive and repulsive interactions are modified and come from the lone pair charges interacting with surface silicon and oxygen atoms, respectively. This gives the structure shown in Figure 5b, where both water hydrogens lie flat in the *xy* plane and there are no hydrogen bonds with the surface. As noted above, somewhat surprisingly given the structural differences, both water models give essentially the same binding energy.

A water molecule binds much more strongly to the Al surface, and the energies that we obtain (Table 1) compare well with previous DFT calculations.[28] Note that when the zero-point energy (not present in our classical model) is removed, the DFT binding energy is ∼−43.4 kJ/mol, which is close to our values (−46.4 kJ/mol for SPC/E and −45.6 kJ/mol for TIP5P-E). The SPC/E model promotes a very attractive interaction between a downward-pointing water hydrogen and a hydroxyl oxygen forming a donor hydrogen bond (Figure 5c). Two additional acceptor hydrogen bonds are formed between the water oxygen and two surface hydroxyl hydrogens, giving a total of three.

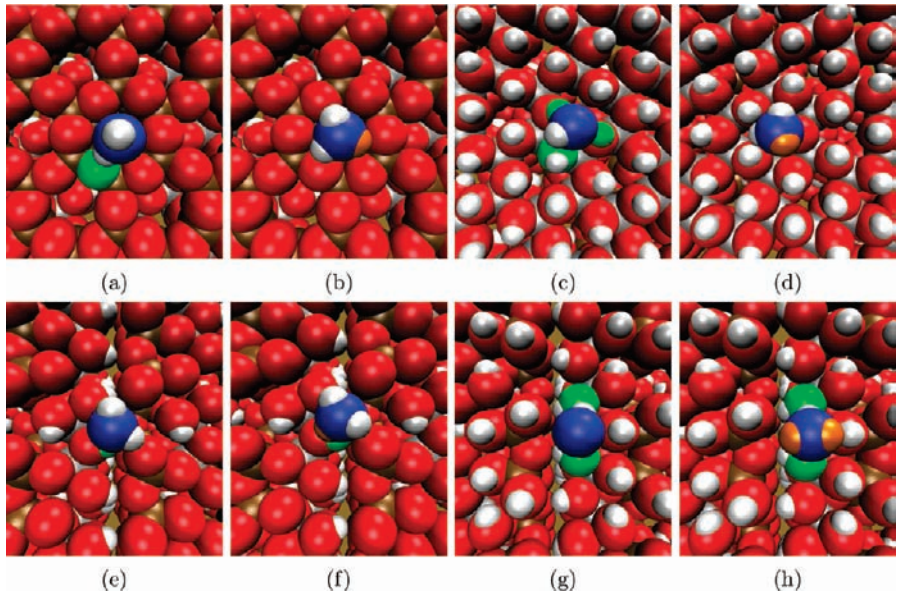

Figure 5. Snapshots of a water molecule at 10 K for the Si surface (a, b), Al surface (c, d), unprotonated edge (e, f), and protonated edge (g, h) using the SPC/E (a, c, e, g) and TIP5P-E (b, d, f, h) water models. The water oxygens are blue, lattice oxygens are red, hydrogens are white, aluminums are gray, silicons are brown, lone pairs are orange, and the surface atoms involved in hydrogen bonding with the water molecule are indicated in green.

The number of hydrogen bonds and the structure shown in Figure 5c are in agreement with the DFT results reported by Hu and Michaelides.[28] The TIP5P-E model gives a somewhat different structure, with the strongest attractive interactions again coming through the lone pair charges. One lone pair forms an acceptor hydrogen bond with a hydroxyl hydrogen and interacts favorably with neighboring underlying aluminum atoms. This gives a structure with the water hydrogens lying flat in the *xy* plane, as shown in Figure 5d. We note that, despite the orientational differences, both models give similar net binding energies. Also, the monolayer structures obtained at higher temperatures, which are clearly influenced by water−water as well as water−surface interactions, are very similar (see Figure 6d). Both low-temperature structures (Figure 5c and d) actually occur in the monolayers obtained at 298 and 235 K, for both water models. However, we note that it is only for the TIP5P-E model that the water−surface interaction is attractive for both configurations, likely explaining the slightly larger adsorption range observed for TIP5P-E.

For both edges, the low-energy water structures occur near the junction between the Si and Al surfaces (Figure 5e and f). For the unprotonated edge, a very favorable interaction is formed between the water oxygen (SPC/E) or lone pairs (TIP5P-E) and a hydroxyl hydrogen from the Al surface, thus forming an acceptor hydrogen bond with both models. Note that, although there are a large number of bare oxygen atoms exposed on the unprotonated edge, no donor hydrogen bonds are observed.

For the protonated edge, the most attractive interactions are formed between the water hydrogens and hydroxyl and bridging oxygens, leading to two donor hydrogen bonds for both models (Figure 5g and h). For both types of edge, the delocalization of the partial negative charge from the center of the water oxygen nucleus (SPC/E) to the lone pair locations (TIP5P-E) has minimal impact on the structures obtained. However, it does give a significant change in the binding energy on the protonated edge, increasing from −94.1 (SPC/E) to −78.5 kJ/mol (TIP5P-E), whereas the energies obtained for the unprotonated edge are very similar. For the protonated edge, the difference is explained by the fact that for the TIP5P-E model, the water−surface interaction is more sensitive to the presence of neighboring, non-hydrogen-bonding surface atoms.

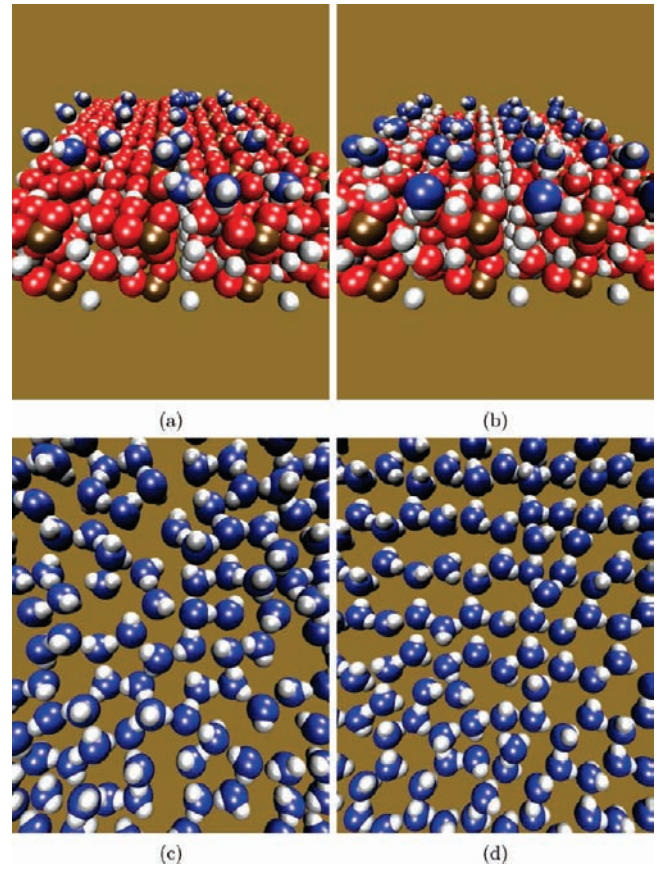

Figure 6. Snapshots obtained at 235 K using the TIP5P-E model for low water coverage on the unprotonated edge (a) and the protonated edge (b) and for monolayer coverage on the unprotonated edge (c) and the Al surface (d). The water oxygens and hydrogens are blue and white, respectively.

C. Water Structure at Monolayer and Submonolayer Coverage. Snapshots obtained for submonolayer coverage on both edges and for monolayer coverage on the unprotonated

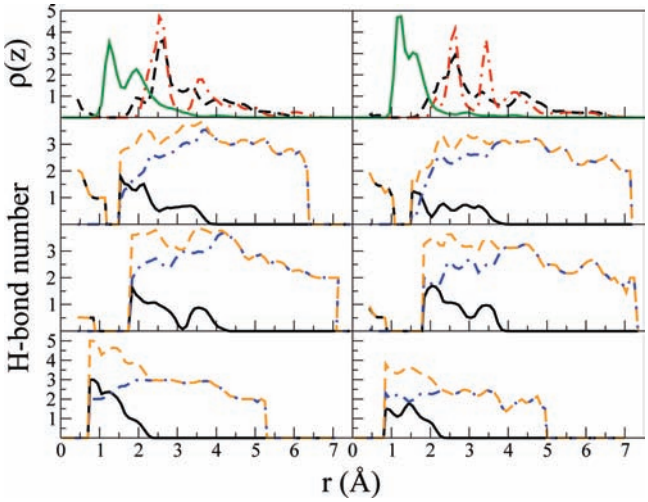

Figure 7. The water density (g/cm^3) profile (topmost panel) and the average number of hydrogen bonds per water molecule at 235 K, obtained for monolayer coverage using the SPC/E (left) and TIP5P-E (right) models. The dashed (black), dotted−dashed (red), and solid (green) lines in the density plot correspond to the unprotonated edge, protonated edge, and Al surface, respectively. The lower three panels give the hydrogen-bond numbers for the Al surface (bottom), protonated edge (middle), and unprotonated edge (top). In these panels, the solid (black), dotted−dashed (blue), and dashed (orange) curves represent water−surface bonds, water−water bonds, and total number, respectively.

edge and the Al surface are shown in Figure 6. These results were obtained for the TIP5P-E model at 235 K. Images obtained for the SPC/E model at 235 K, and for both models at 298 K, are very similar to those given in Figure 6 and hence are not shown. It is evident from Figure 6a and b that, at low coverage, water molecules adsorb on the edges at well-defined binding sites and with particular orientations (as described above).

We note that for both edges and the Al surface, at monolayer coverage, the adsorbed water layer exhibits little order, and no long-range patterns are discernible (Figure 6c and d). A detailed analysis of the nature of the monolayer on the Al surface, and its possible relevance to ice nucleation under atmospheric conditions, was given in a previous communication.[29] To briefly summarize, although some hexagonal structures do form on the Al surface (Figure 6d), the relevant lattice parameter is considerably larger than that required to match ice *Ih*. Structure factors calculated for the surface layer employing reciprocal lattice vectors appropriate for hexagonal ice[59,60] are close to 0. The expected strain on the ice embryo due to this mismatch would depress the nucleation temperature to well below the atmospherically relevant range.[29,61] Therefore, our results do not support the theory that kaolinite serves as a good ice nucleus because the crystallographic properties of kaolinite are such that the Al surface is particularly hospitable to water structures that closely match hexagonal ice.

D. Water Density and Hydrogen Bonding at Monolayer Coverage. Water density profiles, $\rho(z)$, (in g/cm^3) and hydrogen-bond numbers (as functions of z) for monolayer coverage on the Al surface and both edges are plotted in Figure 7. In this figure, $z = 0$ corresponds to the center of the highest surface hydroxyl hydrogen for the Al surface and to the center of the lowest exposed oxygen atom for the edges. We note that the density is quite high near the surfaces, indicating a rather compact layer, and shows some structural features associated with the atomic granularity of the surface.

For each surface, the average total number of hydrogen bonds per water molecule is shown together with the water−surface and water−water contributions. Generally, we see that near the surface, in the most compact region of the layer, water molecules tend to have about four hydrogen bonds, as one would expect, but the number can be a little higher or lower depending on the surface and the particular location. Also, not unexpectedly, there are fewer hydrogen bonds in the outer fringes of the layer. Comparing the average number of water−surface hydrogen bonds in the monolayer with the numbers given in Table 1 for a single water molecule, some differences are noticeable. These differences arise because in the monolayer, interactions with neighboring water molecules strongly influence the geometrical arrangements. This tends to reduce the differences between the water models, giving qualitatively similar monolayer structures, as noted above.

A density and hydrogen bond analysis was also carried out at 298 K. The results obtained were similar to those discussed above, except that the structural features tended to be a little broader and less sharp than those observed at 235 K. This is consistent with the larger fluctuations expected at the higher temperature.

IV. Summary and Conclusions

GCMC simulations have been employed to examine water uptake and structure on the Al surface, the Si surface, and two edge-like surfaces of kaolinite. Simulations were carried out for a range of chemical potentials (vapor pressures) at the atmospherically relevant temperatures, 298 and 235 K. Two water models, the SPC/E and TIP5P-E, were considered. At low temperature (10 K), these models prefer different orientations on some surfaces, but the single-molecule binding energies are in good agreement and, for the Al surface, compare well with earlier DFT calculations.[28] At 298 and 235 K, both models gave similar adsorption isotherms and monolayer structures.

From a modeling perspective, we found that arbitrary truncation of a kaolinite slab along the axis perpendicular to the surface of interest (the z axis in this paper) can lead to unphysical fields far from the surface. These fields can lead to spurious results that strongly depend on where the slab is truncated. We show that this problem can be overcome by simply including two slabs in the simulation cell, oriented such that the unphysical, long-range fields cancel exactly. With this simulation arrangement, the results obtained become quite insensitive to slab thickness.

As previously known,[33] the Si surface is relatively hydrophobic, and at both temperatures considered, we find no significant water adsorption before saturation. The Al surface and both edges take up water and form monolayers before saturation at atmospherically relevant pressures. The edges have by far the greatest affinity for water, adsorbing at very low chemical potentials and up to monolayer coverage. This, together with the fact that edge-like surfaces account for a significant fraction of the total surface area of kaolinite particles,[50,51] suggests that edges might play an important role in heterogeneous surface chemistry, where water is needed for hydrolysis.

The mechanism of water uptake on the edges is distinctly different from that of the Al surface. Adsorption on the edges appears to be driven mainly by strong water−surface interactions. On the edges, water molecules initially adsorb at well-defined periodic binding sites, and the coverage grows essentially continuously with chemical potential until a monolayer is achieved. In contrast, on the Al surface, there is practically no submonolayer adsorption, and monolayer formation appears as a fairly sharp transition. This indicates that collective behavior associated with water−water interactions is essential to monolayer formation on the Al surface. Further evidence for this is

given by the large hysteresis observed on water desorption from the Al surface. Very little hysteresis is observed for the edges.

The monolayer structure on the Al surface and that on both edges was analyzed through density and hydrogen-bond number profiles. The density profiles $\rho(z)$ reached a maximum of 3−5 g/cm^3, depending on the surface, indicating that the monolayers are rather dense. In the dense regions of the monolayers, a water molecule tends to form about four hydrogen bonds, some with the surface and some with other water molecules of the monolayer. The details of the density and hydrogen-bond number profiles do show some variation with the water model employed, but overall, the monolayer structures are very similar.

Finally, we note that for all surfaces considered, at 298 K, we observe only monolayer coverage before saturation (bulk condensation of the vapor). This contrasts with recent experimental results for kaolinite particles,[41] where much higher coverages are reported for relative humidities well below 100%. Our simulations suggest that the experimental observations cannot be explained with atomistically smooth surfaces and that surface roughness likely plays a very important role in water adsorption by kaolinite particles.

Acknowledgment. The financial support of the Natural Science and Engineering Research Council of Canada and the Canadian Foundation for Climate and Atmospheric Science is gratefully acknowledged. This research has been enabled by the use of WestGrid computing resources, which are funded in part by the Canada Foundation for Innovation, Alberta Innovation and Science, BC Advanced Education, and the participating research institutions. WestGrid equipment is provided by IBM, Hewlett-Packard, and SGI.

References and Notes

(1) Bauer, S. E.; Balkanski, Y.; Schulz, M.; Hauglustaine, D. A.; Dentener, F. *J. Geophys. Res., Atmos.* **2004**, *109* (D2).
(2) Lunt, D. J.; Valdes, P. J. *J. Geophys. Res., Atmos.* **2002**, *107* (D23).
(3) Tegen, I.; Harrison, S. P.; Kohfeld, K.; Prentice, I. C.; Coe, M.; Heimann, M. *J. Geophys. Res.-Atm.* **2002**, *107* (D21).
(4) Tegen, I.; Miller, R. *J. Geophys. Res., Atmos.* **1998**, *103* (D20), 25975.
(5) Woodward, S. *J. Geophys. Res., Atmos.* **2001**, *106* (D16), 18155.
(6) Glaccum, R. A.; Prospero, J. M. *Mar. Geol.* **1980**, *37* (3−4), 295.
(7) Cziczo, D. J.; Murphy, D. M.; Hudson, P. K.; Thomson, D. S. *J. Geophys. Res., Atmos.* **2004** *109* (D4).
(8) DeMott, P. J.; Cziczo, D. J.; Prenni, A. J.; Murphy, D. M.; Kreidenweis, S. M.; Thomson, D. S.; Borys, R.; Rogers, D. C. *Proc. Natl. Acad. Sci. U.S.A.* **2003**, *100* (25), 14655.
(9) Eastwood, M. L.; Cremel, S.; Gehrke, C.; Girard, E.; Bertram, A. K. *J. Geophys. Res., Atmos.* **2008**, *113*.
(10) Dymarska, M.; Murray, B. J.; Sun, L.; Eastwood, M. L.; Knopf, D. A.; Bertram, A. K. *J. Geophys. Res., Atmos.* **2006**, *111*, D4.
(11) Zuberi, B.; Bertram, A. K.; Cassa, C. A.; Molina, L. T.; Molina, M. J. *Geophys. Res. Lett.* **2002**, *29* (10).
(12) Twohy, C. H.; Kreidenweis, S. M.; Eidhammer, T.; Browell, E. V.; Heymsfield, A. J.; Bansemer, A. R.; Anderson, B. E.; Chen, G.; Ismail, S.; DeMott, P. J.; Van den Heever, S. C. *Geophys. Res. Lett.* **2009**, *36*.
(13) Twohy, C. H.; Poellot, M. R. *Atmos. Chem. Phys.* **2005**, *5*, 2289.
(14) Forster, P.; Ramaswamy, V.; Artaxo, P.; Berntsen, T.; Betts, R.; Fahey, D. W.; Haywood, J.; Lean, J.; Lowe, D. C.; Myhre, G.; Nganga, J.; Prinn, R.; Raga, G.; Schulz, M.; Dorland, R. V. Changes in Atmospheric Constituents and in Radiative Forcing. In *Climate Change 2007: The Physical Science Basis*, Contribution of Working Group I to the Fourth Assessment Report of the Intergovernmental Panel on Climate Change; Solomon, S., Qin, D., Manning, M., Chen, Z., Marquis, M., Averyt, K. B., Tignor, M., Miller, H. L., Eds.; Cambridge University Press: Cambridge, U.K., 2007, pp 129−234.
(15) Cantrell, W.; Heymsfield, A. J. *Bull. Am. Meteor. Soc.* **2005**, *86* (6), 795.
(16) Usher, C. R.; Michel, A. E.; Grassian, V. H. *Chem. Rev.* **2003**, *103* (12), 4883.
(17) Mogili, P. K.; Kleiber, P. D.; Young, M. A.; Grassian, V. H. *Atmos. Environ.* **2006**, *40* (38), 7401.
(18) Mashburn, C. D.; Frinak, E. K.; Tolbert, M. A. *J. Geophys. Res., Atmos.* **2006**, *111* (D15).
(19) Goodman, A. L.; Bernard, E. T.; Grassian, V. H. *J. Phys. Chem. A* **2001**, *105* (26), 6443.
(20) Krueger, B. J.; Ross, J. L.; Grassian, V. H. *Langmuir* **2005**, *21* (19), 8793.
(21) Hanisch, F.; Crowley, J. N. *Phys. Chem. Chem. Phys.* **2001**, *3* (12), 2474.
(22) Laskin, A.; Wietsma, T. W.; Krueger, B. J.; Grassian, V. H. *J. Geophys. Res., Atmos.* **2005**, *110* (D10).
(23) Santschi, C.; Rossi, M. J. *J. Phys. Chem. A* **2006**, *110* (21), 6789.
(24) Tunega, D.; Gerzabek, M. H.; Lischka, H. *J. Phys. Chem. B* **2004**, *108*, 5930.
(25) Tunega, D.; Benco, L.; Haberhauer, G.; Gerzabek, M. H.; Lischka, H. *J. Phys. Chem. B* **2002**, *106*, 11515.
(26) Tunega, D.; Haberhauer, G.; Gerzabek, M. H.; Lischka, H. *Langmuir* **2002**, *18*, 139.
(27) Hu, X. L.; Michaelides, A. *Surf. Sci.* **2007**, *601*, 5378.
(28) Hu, X. L.; Michaelides, A. *Surf. Sci.* **2008**, *602*, 960.
(29) Croteau, T.; Bertram, A. K.; Patey, G. N. *J. Phys. Chem. A* **2008**, *12*, 10708.
(30) Pruppacher, H. R.; Klett, J. D. *Microphysics of Clouds and Precipitation*, 2nd rev. ed.; Kluwer Academic: Dordrecht, The Netherlands, 1997; pp 329−331.
(31) Warne, M. R.; Cosgrove, T. *Phys. Chem. Chem. Phys.* **2000**, *2*, 3663.
(32) Vasconcelos, I. F.; Bunker, B. A.; Cygan, R. T. *J. Phys. Chem. C* **2007**, *111*, 6753.
(33) Delville, A. *J. Phys. Chem.* **1995**, *99*, 2033.
(34) Wassermann, B.; Reif, J.; Matthias, E. *Phys. Rev. B* **1994**, *50*, 2593.
(35) Shevkunov, S. V. *Colloidal J.* **2005**, *67*, 497.
(36) Shevkunov, S. V. *Colloidal J.* **2007**, *69*, 360.
(37) Taylor, J. H.; Hale, B. N. *Phys. Rev. B* **1993**, *47*, 9732.
(38) Cerdá, J.; Michaelides, A.; Bocquet, M.-L.; Feibleman, P. J.; Mitsui, T.; Rose, M.; Fomin, E.; Salmeron, M. *Phys. Rev. Lett.* **2004**, *93*, 116101–1.
(39) Michaelides, A.; Morgenstern, K. *Nat. Mater.* **2007**, *6*, 597.
(40) Nutt, D. R.; Stone, A. J. *Langmuir* **2004**, *20*, 8720.
(41) Schuttlefield, J. D.; Cox, D.; Grassian, V. H. *J. Geophys. Res.* **2007**, *112*, D21303.
(42) Cygan, R. T.; Liang, J.-J.; Kalinichev, A. G. *J. Phys. Chem. B* **2004**, *108*, 108–1255.
(43) Berendsen, H. J. C.; Postma, J. P. M.; van Gunsteren, W. F.; Hermans, J. In *Intermolecular Forces*; Pullman, B., Ed.; Reidel: Dordrecht, The Netherlands, 1981; p 331.
(44) Bish, D. L. *Clays Clay Miner.* **1993**, *41*, 783.
(45) Berendsen, H. J. C.; Grigera, J. R.; Straatsma, T. P. *J. Phys. Chem.* **1987**, *91*, 6269.
(46) Lisal, M.; Nezbeda, I.; Smith, W. R. *J. Phys. Chem. B* **2004**, *108*, 7412.
(47) Mahoney, M. W.; Jorgensen, W. L. *J. Chem. Phys.* **2000**, *112*, 8910.
(48) van der Spoel, D.; van Maaren, P. J.; Berendsen, H. J. C. *J. Chem. Phys.* **1998**, *108*, 10220.
(49) Vega, C.; Sanz, E.; Abascal, J. L. *J. Chem. Phys.* **2005**, *122*, 114507.
(50) Brady, P. V.; Cygan, R. T.; Nagy, K. L. *J. Colloid Interface Sci.* **1996**, *183*, 356.
(51) Zbik, M.; Smart, R. S. C. *Clays Clay Miner.* **1998**, *46* (2), 153.
(52) Wang, Y.-S.; Siu, W.-K. *Can. Geotech. J.* **2006**, *43*, 587.
(53) Shelley, J. C.; Patey, G. N. *Mol. Phys.* **1996**, *88*, 385.
(54) Yeh, I.-C.; Berkowitz, M. L. *J. Chem. Phys.* **1999**, *111*, 3155.
(55) Allen, M. P.; Tildesley, D. J. *Computer Simulation of Liquids*; Oxford: New York, 1987.
(56) Shelley, J. C.; Patey, G. N. *J. Chem. Phys.* **1995**, *102*, 7656.
(57) (a) Luzar, A.; Chandler, D. *Nature* **1996**, *53*, 379. (b) Luzar, A.; Chandler, D. *Phys. Rev. Lett.* **1996**, *76*, 928.
(58) Luzar, A. *J. Chem. Phys.* **2000**, *113*, 10663.
(59) Kittel, C. *Introduction to Solid State Physics*, 2nd ed.; Wiley & Sons, Inc.: New York, 1953.
(60) Kroes, G. J. *Surf. Sci.* **1992**, *275*, 365.
(61) Turnbull, D.; Vonnegut, B. *Ind. Eng. Chem.* **1952**, *44*, 1292.

JP902453F